Auxetic Liquid Crystal Vitrimers with Adjustable Poisson's Ratios Enabled by Topological Rearrangements of Polymer Network

Zhiran Zheng, Weixin Ma, Jiawei Li, Yaning Ma, Jun Hu, Min-hui Li

Auxetic liquid crystal vitrimers with adjustable Poisson's ratios enabled by topological rearrangements of polymer network

Zhiran Zheng, Weixin Ma, Jiawei Li, Yaning Ma, Jun Hu and Min-Hui Li**

Z. Zheng, W. Ma, J. Li, Y. Ma, J. Hu
Beijing Advanced Innovation Center for Soft Matter Science and Engineering, Beijing University of Chemical Technology, North Third Ring Road 15, Chaoyang District, Beijing 100029, China
E-mail: jhu@mail.buct.edu.cn

J. Hu
State Key Laboratory of Polymer Physics and Chemistry, Changchun Institute of Applied Chemistry, Chinese Academy of Sciences, Renmin Street 5625, Chaoyang District, Changchun 130022, China

M.-H. Li
Chimie ParisTech, PSL University, CNRS, Institut de Recherche de Chimie Paris, 11 rue Pierre et Marie Curie, Paris 75005, France
E-mail: min-hui.li@chimieparistech.psl.eu

Keywords: metamaterials, liquid crystal elastomer, dynamic covalent bonds, negative Poisson's ratio, auxetic effect

Metamaterials feature extraordinary physical properties that break the cognitive limitations of human beings on traditional materials. Auxetic materials and liquid crystal elastomers (LCEs) are representative of typical mechanical and thermal metamaterials. Their combination may introduce some unconventional and counterintuitive performances. Nevertheless, studies on LCEs with negative Poisson's ratio (ν) are still rare. Herein, we develop a liquid crystal vitrimer (Poly-LCE) that is a polydomain main-chain LCE containing dynamic ester bonds. Its orientation process to monodomain (Mono-LCE) is greatly simplified by transesterification reaction-induced topological network rearrangement under mechanical alignment. By optimizing geometric parameters of re-entrant (R) structures and orientation of liquid crystal units, all samples of R-Poly-LCE, R-Mono-LCE (//), and R-Mono-LCE (⊥) show negative

Poisson's ratio (NPR) below 2% elongation (ν = -0.22 ~ 0 for R-Poly-LCE, ν = -0.12 ~ 0 for R-Mono-LCE (//) and ν = -0.16 ~ 0 for R-Mono-LCE (⊥)). Interestingly, R-Poly-LCE presents $\nu > 0$ within 2% - 10% axial elongation, while R-Mono-LCE (//) and R-Mono-LCE (⊥) exhibit $\nu \approx 0$ under the same elongation. Materials with negative and zero Poisson's ratios are interesting in niche applications. This work develops a simple method to prepare these materials by liquid crystal vitrimers.

1. Introduction

Metamaterials are characterized by their negative index, for example, by negative Poisson's ratio (NPR) when mechanical metamaterials are discussed.[1] Metamaterials exhibit extraordinary physical properties because of their specific molecular or atomic arrangements or macroscopic geometric structures.[2-4] Their unique performances break the cognitive limitations of human beings on traditional materials.[5, 6] Among them, mechanical metamaterials (also named auxetic materials) are the most reported ones,[7, 8] which expand laterally when being stretched, or contract laterally when being compressed,[9-12] and therefore possess NPR effect.[13-15] Auxetic materials have shown great potential in various applications, such as energy adsorption, deployable devices, and robotic systems. In the last two decades, thermal metamaterials that contract upon heating (expand upon cooling) and exhibit intrinsic negative thermal expansion (NTE) have also been an attractive topic in solid-state chemistry.[1, 16, 17] Interestingly, a soft material, aligned liquid crystalline elastomer (simply noted as LCE hereinafter), can also be considered as a thermal metamaterial by excellence, which exhibits 1D NTE along the direction of orientation.[18-20] LCEs are moderately crosslinked LC polymers, where LC units and polymer chains are oriented uniformly in the whole sample (monodomain). The key characteristic of monodomain LCEs that combine the order of LC with the elasticity of rubbers is they have the capability to contract unidirectionally, reversibly, and largely (typical strain of 20 – 200%) upon heating across the LC-isotropic phase transition due to the reversible variation of the LC order and chain conformation.[21,22] Moreover, the heating can be driven by other thermal modes, such as photothermal and electrothermal modes.[23-25] Very recently, researchers attempt to combine NPR and NTE properties in the same LCE to generate cross-metamaterials with unconventional and even counterintuitive performance.[26-34] For example, Gleeson et al. reported for the first time a nonporous molecular auxetic LCE with special LC moieties.[29, 32] Zhao et al. observed unconventional 2D NTE in a mechanically stretched monodomain LCE: across its LC-isotropic phase transition, both the LCE length and width contracted in isotropic phase, and elongated in LC phase.[30] In most of these auxetic materials, geometric structures likely to get NPR, such as re-entrant porous lattice structures,

were created in LCEs.[26-28, 31, 33, 34] The advantage of using LCE is the possibility to modulate Poisson's ratio by graded LCEs with different alignments and by temperature in a fixed geometry.[26] This possibility to obtain the distributed negative and positive Poisson's ratios may be important in real applications, such as in biological implants.[35, 36] Nevertheless, as far as we are aware, there is only one report that describes LCE lattices with a fixed geometry that exhibits adjustable Poisson's ratios.[26] Other works actually only described 2D NTE.[27,28, 31, 33, 34] Therefore, the development of auxetic LCEs with adjustable NPR is relevant and important. In this work, we have developed LCEs with re-entrant lattice structures whose beams have various alignments including polydomain (non-oriented) and monodomain with parallel and perpendicular orientation direction (**Scheme 1**). More specifically, for the easy and fast achievement of different alignments, dynamic covalent bonds are introduced in LCE system, which allows to manipulate the alignment from a polydomain LCE (Poly-LCE) by topological network rearrangements.[37-39] In addition, the dynamic bond exchange reaction makes LCEs recyclable and weldable.[40, 41] Therefore, auxetic liquid crystal vitrimers with adjustable NPR were actually developed.

A main-chain Poly-LCE containing dynamic ester bonds was first synthesized from diglycidyl ether of 4, 4′-dihydroxybiphenol (DGE-DHBP) and hexadecane diacid (Scheme 1, Scheme S1, Supporting Information). Due to topological network rearrangements induced by transesterification reactions (TERs), the orientation process from Poly-LCE to monodomain LCE (Mono-LCE) can be performed readily to obtain Mono-LCE with parallel or perpendicular orientation relative the stretching direction, noted as Mono-LCE (//) or Mono-LCE (⊥). After laser cutting, LCE with re-entrant lattice (R), noted as R-Poly-LCE, R-Mono-LCE (//), and R-Mono-LCE (⊥) were finally obtained (Table S1, Supporting Information). All samples of R-Poly-LCE, R-Mono-LCE (//), and R-Mono-LCE (⊥) with a beam of width 1.4 mm, re-entrant angle of 120^{o}, and array units of 6×7 show NPR below the elongation of 2%. Very interesting, R-Poly-LCE presents $\nu > 0$ when axial elongation ratio is from 2% to 10%, while R-Mono-LCE (//) and R-Mono-LCE (⊥) exhibit $\nu \approx 0$ under 2% to 10% stretching. Materials with zero Poisson's ratios, existing in natural materials, are also interesting in niche applications. For example, cork is a near-zero Poisson's ratio material that does not dilate or contract on compression; wings of beetles also have near zero Poisson's ratio.[42, 43] Additionally, energy-absorbing materials in aerospace field, variant cars with reduced drag requirements, as well as medical dressings with good human shape in medical field, also require materials with near-zero Poisson's ratio. This work pioneeringly addresses the following issues: 1) Exploring a universal law for reducing the Poisson's ratio of main-chain LCEs through synergistic control

via geometric parameters and arrangements of liquid crystal units using a relatively conventional molecular chain design; 2) Providing insights for structured main-chain LCEs that exhibit auxetic behavior only within a narrow deformation range post-cutting, and indicating that the occurrence range of zero Poisson's ratio can be further expanded through stretching orientation. By ingeniously combining dynamic chemistry with the structured laser cutting, we not only simplify the orientation process of LCE by topological network rearrangement, but also introduce a non-uniform control method to alter material's Poisson's ratio in a wide range, offering a flexible preparation strategy that extends the use of dynamic covalent bonds in the field of metamaterials.

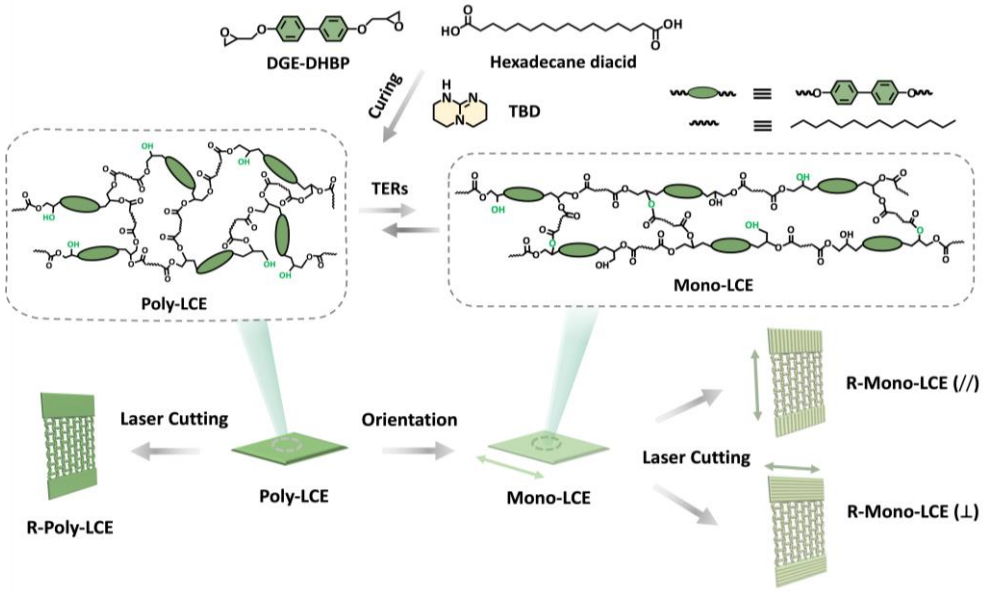

Scheme 1. Schematic illustration for the elaboration of Poly-LCE and Mono-LCE using topological network rearrangements, followed by the subtraction manufacturing for R-Poly-LCE, R-Mono-LCE (//), and R-Mono-LCE (⊥) using laser cutting. Green arrows indicate the orientation direction by stretching.

2. Results and Discussion

2.1. Poly-LCE preparation and their mesomorphic and dynamic properties

Prior to the preparation of Poly-LCE, the monomer DGE-DHBP was synthesized from 4, 4-dihydroxy biphenyl (4, 4-DB) and epichlorohydrin (ECH), and purified thrice by recrystallization (Figure S1, Supporting Information). ^{1}H-NMR spectrum clearly identified the characteristic proton peaks of DGE-DHBP, confirming the successful synthesis (Figure S2, Supporting Information). The monomer DGE-DHBP only showed crystalline phases with melting temperature T_m = 155°C and recrystallization temperature T_{cr} = 146°C (Figure S3, Supporting Information), indicating that there was no liquid crystal phase in DGE-DHBP.[44]

After reacting DGE-DHBP with hexadecane diacid in the presence of the catalyst 1,5,7-triazabicyclo[4.4.0]dec-5-ene (TBD) in a plate vulcanizing machine under 180°C for 4 h, a smooth main-chain liquid crystal elastomer (Poly-LCE) was obtained (**Figure 1**a). Poly-LCE only swelled but didn't dissolve at room temperature in most organic solvents (trichlorobenzene, chloroform, tetrahydrofuran, acetonitrile, and ethanol), in which its gel content was measured as over 83% (Table S2, Supporting Information). Therefore, the crosslinked networks were actually formed in Poly-LCE. Even though the monomer DGE-DHBP was not mesomorphous, Poly-LCE exhibited a liquid crystal phase with transition temperatures peaks at $T_{LC\text{-}iso}$ = 116°C on heating and $T_{iso\text{-}LC}$ = 101°C on cooling according to DSC (Figure 1b). Its glass transition temperature (T_g) was also measured at 52°C on heating. Poly-LCE was further characterized by dynamic mechanical analysis (DMA) (Figure 1c). The storage modulus *G* gradually decreased with the increasing temperature, and there were two peaks in tan (δ) curve at 55 °C and 110 °C, corresponding to T_g and $T_{LC\text{-}iso}$ of Poly-LCE, respectively. The difference in T_g and $T_{LC\text{-}iso}$ measured by DSC and DMA was within a reasonable range. 2D wide-angle X-ray scattering (WAXS) pattern with two isotropic rings indicated that Poly-LCE was polydomain and not aligned (Figure 1d). The inner ring signal with peak position at q_{peak} = 0.42 $Å^{-1}$ revealed a smectic phase with layer spacing of 15.0 Å, while the outer ring signal with peak position at q_{peak} = 1.36 $Å^{-1}$ corresponded to an average lateral distance between two biphenyl monomers of 4.6 Å. The observation by polarizing microscopy (POM) also confirmed the birefringence of liquid crystal phase without alignment of Poly-LCE (Figure 1e). Generally, the shaping or recovery temperature used to characterize shape memory performance was more than 15°C above the phase transition temperature. Thus, 70°C (above T_g) and 150°C (above $T_{LC\text{-}iso}$) were selected for the triple shape memory performance, which confirmed that Poly-LCEs could transform its original shape according to different temperature thresholds (Figure S4, Supporting Information).

In Poly-LCE, ester bonds can break and recombine at the temperature above the activation barrier, inducing topological network rearrangements and releasing external stress.[45] The mechanism of topological network rearrangements induced by TERs was briefly shown in Scheme 1. Free hydroxyl groups in Poly-LCE networks attacked ester bonds to generate new hydroxyl groups and ester bonds, causing the occurrence of topological rearrangements of the crosslinked networks. The stress relaxation curves obtained by DMA (Figure 1f) showed that the relaxation time (τ^*) of Poly-LCE, defined as the time when the storage modulus of Poly-LCE relaxed to 1/e of the initial one (G/G_0 = 1/e) was 5500 s at 140 °C, 2500 s at 160 °C, and

only 400 s at 200 °C. This result followed a Maxwell model fitted by an Arrhenius equation (1):[45]

$$ln\tau^* = \frac{E_a}{RT} - lnA\ldots\ldots(1)$$

where τ^*, E_a, T, and R represent the relaxation time, activation energy of TERs, temperature, and universal gas constant, respectively. As shown in Figure S5a (Supporting Information), the E_a was calculated to be 75 kJ mol^{-1}, consistent with the E_a of TERs reported by Leibler and other groups (69~150 kJ mol^{-1}).[45, 46, 47] Moreover, the malleability temperature (T_{mall}) for Poly-LCE was measured by thermodilatometry test, which is instructive for topological network rearrangements and great helpful to guide the dynamic processing like recycling and welding (Figure S5b, Supporting Information).[48,49] A notable increase in the expansion strain was observed at 180°C that was defined as T_{mall}. Below 180ºC, Poly-LCE behaved as an ordinary thermoset due to the relatively slow TERs. On the contrary, above 180ºC, the rapid TERs endowed the network with a certain fluidity.[39] Thanks to the dynamic properties of Poly-LCE, it enabled recycling and welding. By collecting the broken and discarded Poly-LCE and re-pressing them on a hot tablet at T = T_{mall} = 180ºC for 4 h, a neat piece of the recycled Poly-LCE can be obtained (Figure 1g). In addition, after superimposing two strips of Poly-LCE in an oven at 180ºC for 1 h, they fused into one strip through TERs, which could bear a weight of 1200 times its own gravity (Figure 1h), demonstrating the weldable property of Poly-LCE. In short, Poly-LCE is a liquid crystal vitrimer whose dynamic ester bonds will allow to perform topological rearrangement inside the sample for further manipulation of LC polymer orientation as discussed in the following section.

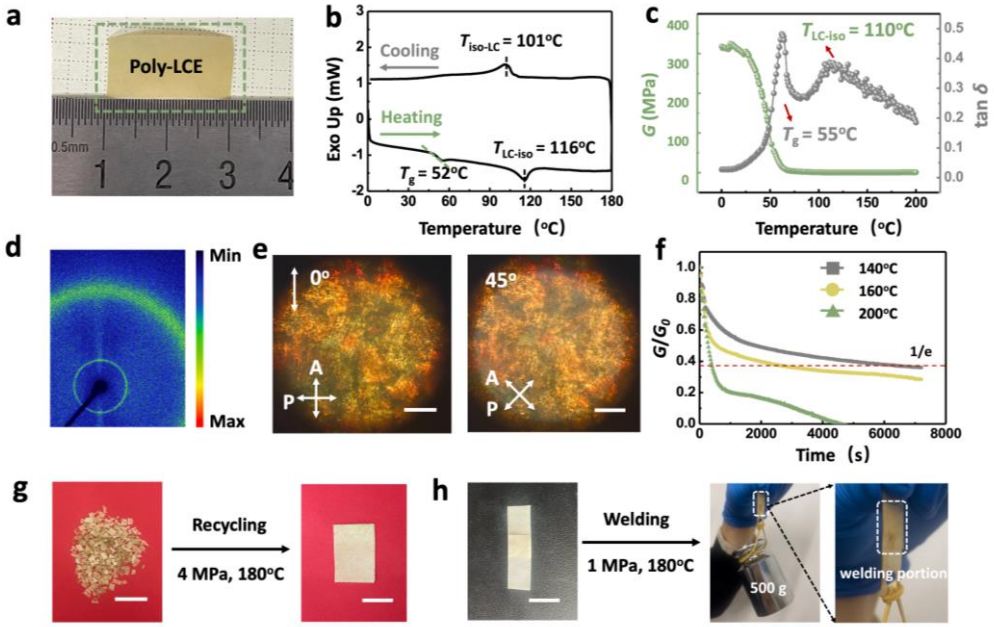

Figure 1. Preparation and characterization of Poly-LCE. a) Photograph of a Poly-LCE film. b) DSC curves of Poly-LCE between 0 and 180°C at a heating/cooling rate of 5°C min^{-1}. c) Storage modulus *G* and loss angle tangent tan δ of Poly-LCE as a function of temperature from 0 to 200°C under a heating rate of 5°C min^{-1} measured by DMA. d) 2D WAXS diagram of Poly-LCE (from 0.001 to 2.25 $Å^{-1}$ of $q = (4\pi \sin \theta)/\lambda$). The ring signals with peak positions at q_{peak} = 0.42 $Å^{-1}$ and 1.36 $Å^{-1}$ correspond to the smectic layer spacing of 15.0 Å and the average lateral distance between two biphenyl units of 4.6 Å. e) Texture of Poly-LCE under POM at two orientations relative to polarizer at room temperature after cooling from isotropic phase. Scale bar: 20 μm. Sample thickness: 0.1 mm. f) Stress relaxation of Poly-LCE at 140 °C, 160 °C, and 200 °C using DMA tension mode with a strain of 5%. g) Physical recycling, and h) welding of Poly-LCE at 180°C. Scale bar was 1 cm in g) and h).

2.2. Preparation of Mono-LCE from Poly-LCE through TERs-induced topological network rearrangements

Benefiting from the dynamic nature of the networks, the orientation of liquid crystal elements can be achieved through the TERs-induced topological network rearrangements in Poly-LCE under mechanical stretching, and Mono-LCE can be eventually obtained.[39] During this process, Poly-LCE was heated by a hot fan and uniaxially stretched by a self-made mold to reach the temperature of TERs and to perform the alignment (Figure S6, Supporting Information). Briefly, Poly-LCE of 0.2 mm thickness was heated to 180°C, at which the crosslinked network was rearranged by TERs and showed a certain fluidity like a thermoplastic. It was then stretched to 20%-140% of its original length and maintained for 30 s. Then the sample under stretching was cooled to 120°C just above T_i, annealed at 120°C for 10 min, and cooled down to room temperature (25°C). Consequently, the orientation of Poly-LCE was achieved and permanently retained to get Mono-LCE. The resulting Mono-LCE showed typical thermoactive reversible contraction when heated from room temperature (25°C) to isotropic phase (120°C) (**Figure 2**a). The contraction ratio was calculated as $(L_0–L_{iso})/L_0$, where L_0 was the original length of Mono-LCE at room temperature and L_{iso} was the length at isotropic phase. The pre-strain (strain used in the preparation of Mono-LCE by stretching) is a key parameter affecting the reversible contraction ratio. When the pre-strain increased from 0% to 80%, the higher the pre-strain, the greater the reversible contraction ratio. When the pre-strain was 80%, the maximal contraction was 68%. Once the pre-strain exceeded 80% until 140%, the reversible contraction ratio didn't increase further (Figure 2b). Therefore, 80% was selected as the pre-strain for alignment to prepare Mono-LCE in the following discussion unless otherwise stated. This is due to when the strain is less than 80%, the chaotic arrangement caused by the incomplete orientation between

liquid crystal and polymer chain will affect the stability of Poisson's ratio experiment. When the strain is higher than 80%, liquid crystal units have been completely oriented, which is same as the arrangement of liquid crystal units at pre-strain of 80%.

The oriented structure of Mono-LCE was confirmed by POM. When the orientation direction of sample was parallel to the direction of polarizer A, the POM image was dark; while the orientation direction of sample was at an angle of 45° relative to the direction of polarizer A, the image was bright (Figure 2c). 2D WAXS (Figure 2d) further proved the aligned LC phase. The pair of sharp signals at q = 0.43 $Å^{-1}$ along the meridian (the LCE orientation direction) revealed a smectic A phase of layer spacing of 14.6 Å in the sample. To evaluate the effect of orientation direction on mechanical performance, Mono-LCE (//) and Mono-LCE (⊥) were prepared, the long side of which was parallel or perpendicular to the orientation direction (Figure S7, Supporting Information). Tensile stress-strain curves (with stress applied along the long side of sample stripe) showed that Young's modulus of Poly-LCE, Mono-LCE (//), and Mono-LCE (⊥) was 880, 1400, and 640 MPa, respectively (Figure 2e and 2f). The fracture strength and elongation at the break of Poly-LCE were 32.5 MPa and 136%; they were 66.4 MPa and 28% for Mono-LCE (//), and 18.2 MPa and 12% for Mono-LCE (⊥). Interestingly, for Poly-LCE a large stress plateau (with strain from 5% to 100%) was observed after a classical rubber elasticity and before re-hardening and breaking, which corresponded to the soft elasticity of Poly-LCE.[50, 51] The mechanical deformation of aligned LCEs is also highly anisotropic.[52] In the case of Mono-LCE (//) where the monodomain LCE was stretched parallel to the LC director, the stress-strain curve was linear and described by classical rubber elasticity (Young's modulus of 1400 MPa) followed by a narrow pseudo-plateau before breaking. In the case of Mono-LCE (⊥) where the monodomain LCE was stretched perpendicular to the LC director, much lower Young's modulus and breaking stress and strain were observed. These phenomena are similar to those observed in covalently LCE.[50-53] It is worth mentioning that, thanks to the reversible interactions facilitated by dynamic ester bond,[54-56] the recycling process can restore the orientation of liquid crystal units, thereby reverting the material to its isotropic state. The recycled Poly-LCE maintained similar mechanical properties to the original one (Figure S8, Supporting Information).

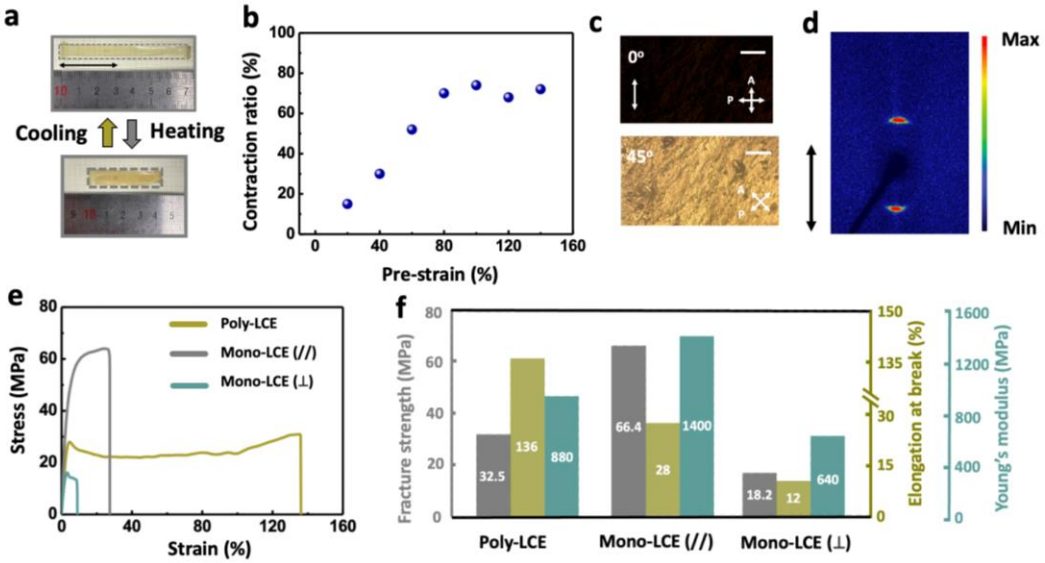

Figure 2. a) Photographs of Mono-LCE (thickness: 0.2 mm) at room temperature (25°C) and its contracted state in the isotropic phase (120°C), thermoactive contraction ratio being 40%. b) The effect of pre-strain (20-140%) on the reversible thermoactive contraction ratio of Mono-LCE with a thickness of 0.2 mm when heated from room temperature (25°C) to isotropic phase (120°C). c) POM images of Mono-LCE with LC orientation direction placed at 0° and 45° relative the polarizer. Sample thickness: 0.1 mm. Scale bar: 500 μm. d) 2D WAXS diagram of Mono-LCE measured at q from 0.001 to 2.25 $Å^{-1}$. q = $(4\pi \sin \theta)/\lambda$. e) Tensile stress-strain curves of Poly-LCE, Mono-LCE (//), and Mono-LCE (⊥) with a 500 N load cell at a stretching rate of 10 mm min^{-1}. f) Young's modulus, fracture strength, and elongation at break of Poly-LCE, Mono-LCE (//), and Mono-LCE (⊥) obtained from tensile stress-strain curves. Double arrows in a), c) and d) indicate the orientation direction of LCE.

2.3. Geometric structure optimization of R-Poly-LCE

Among complex auxetic structures, the re-entrant structure is a typical one where, when the ribs are forced to move outward under a tensile load in the horizontal direction, it expands along the vertical direction.[5, 57-59] As geometric parameters including beam width *w*, re-entrant angle α, and array of units $m \times n$ play key roles in the deformation of re-entrant structure, their effects on auxetic property of R-Poly-LCE in tensile mode were studied. We firstly regulated the *w* as 1.0, 1.4, and 1.8 mm, while keeping a re-entrant angle of 120° and an array of units 6×7 (**Figure 3**a). Tensile stress-strain tests demonstrated that the structural failure strength was 3.8, 5.6, and 11.0 MPa for R-Poly-LCE-1.0mm, R-Poly-LCE-1.4mm, and R-Poly-LCE-1.8mm, respectively, accompanied with the effective deformation value (EDV) before structural failure of 4%, 10%, and 12% (Figure S9, Supporting Information). Within the EDV, the Poisson's ratio (ν) can be deduced in Figure 3b, where the auxetic effect was observed over an extended strain window

for structures. For R-Poly-LCE-1.0mm, the *v* was in the range from -0.25 to 0.18 within EDV from 0 to 4%. When *w* was set to be 1.4 and 1.8 mm, the *v* varied from -0.22 ~ 0.40 for R-Poly-LCE-1.4mm within EDV from 0 to 10%, while -0.16 ~ 0.52 for R-Poly-LCE-1.4mm within EDV from 0 to 12%. Due to the difference in the amount of material being cut, the auxetic effect of re-entrant structure gradually weakened with *w* varying from 1.0 to 1.8 mm, while the mechanical properties integrally increased. It is known that good auxetic behavior is guaranteed by a relatively low Poisson's ratio with a large EDV.[60] In terms of the comprehensive consideration of the minimum *v*, the EDV, and the structural failure strength, R-Poly-LCE-1.4mm was identified to have better auxetic behavior than R-Poly-LCE-1.0mm and R-Poly-LCE-1.8mm (Figure 3c). With mesh size options of R-LCE (Figure S10a, Supporting Information), the finited element analysis (FEA) results confirmed a similar conclusion with experiments (Figure S10b, Supporting Information). As such, the beam width of 1.4 mm was selected.

With beam width fixed at 1.4 mm, the re-entrant angle α from 60^o to 120^o and 150^o were tested while keeping the array of units of 6×7 (Figure 3d). The EDV was 5%, 10%, and 11% with the structural failure strength of 2.4, 5.6, and 5.2 MPa for R-Poly-LCE-60^o, R-Poly-LCE-120^o, and R-Poly-LCE-150^o, respectively (Figure S11, Supporting Information). Accordingly, their *v* ranges were -0.42 ~ 0.10, -0.22 ~ 0.40, and -0.14 ~ 0.52 (Figure 3e). Because of the frozen polymer chains, R-Poly-LCE-60^o needed to overcome greater torsional resistance during the axial tensile, thus was more brittle with fracture at 5% (v_{min} = -0.42). With α increasing to 120^o and 150^o, the EDV enlarged to 10% and 11%, while the auxetic effect weakened (v_{min} = -0.22 for R-Poly-LCE-120^o and v_{min} = -0.14 for R-Poly-LCE-150^o) (Figure 3f). The results of FEA further confirmed this tendency (Figure S12, Supporting Information). According to the comprehensive criteria of good auxetic effect mentioned above, 120^o was selected as the re-entrant angle.

Finally, the array of units was optimized with the beam width of 1.4 nm and the re-entrant angle of 120^o (Figure 3g). As the unit number increased from 6×7 to 6×13 and 6×19, the structural failure strength declined from 5.6 to 4.0 and 1.5 MPa, the EDV decreased from 10% to 7% and 5%, while the minimum *v* was kept approximately constant at -0.22 (Figure 3h; Figure S13, Supporting Information). Similarly, FEA obtained consistent simulation results (Figure S14, Supporting Information). Therefore, 6×7 was chosen as the array of units for the reasons mentioned above (Figure 3i).

In conclusion, the optimal re-entrant structure of R-Poly-LCE possessed the geometric parameters of beam width *w* of 1.4 nm, re-entrant angle α of 120^o, and unit arrays of 6×7.

Certainly, compared with Poly-LCE, the mechanical property of R-Poly-LCE was largely reduced (fracture strength of 5.2 MPa at an elongation of 88% for R-Poly-LCE versus the values of 32.5 MPa and 136% for Poly-LCE) due to the subtraction manufacturing by laser cutting (Figure S15, Supporting Information). Note that the recycled splines of R-Poly-LCE still maintained auxetic performance similar to that of the original sample (Figure S16, Supporting Information).

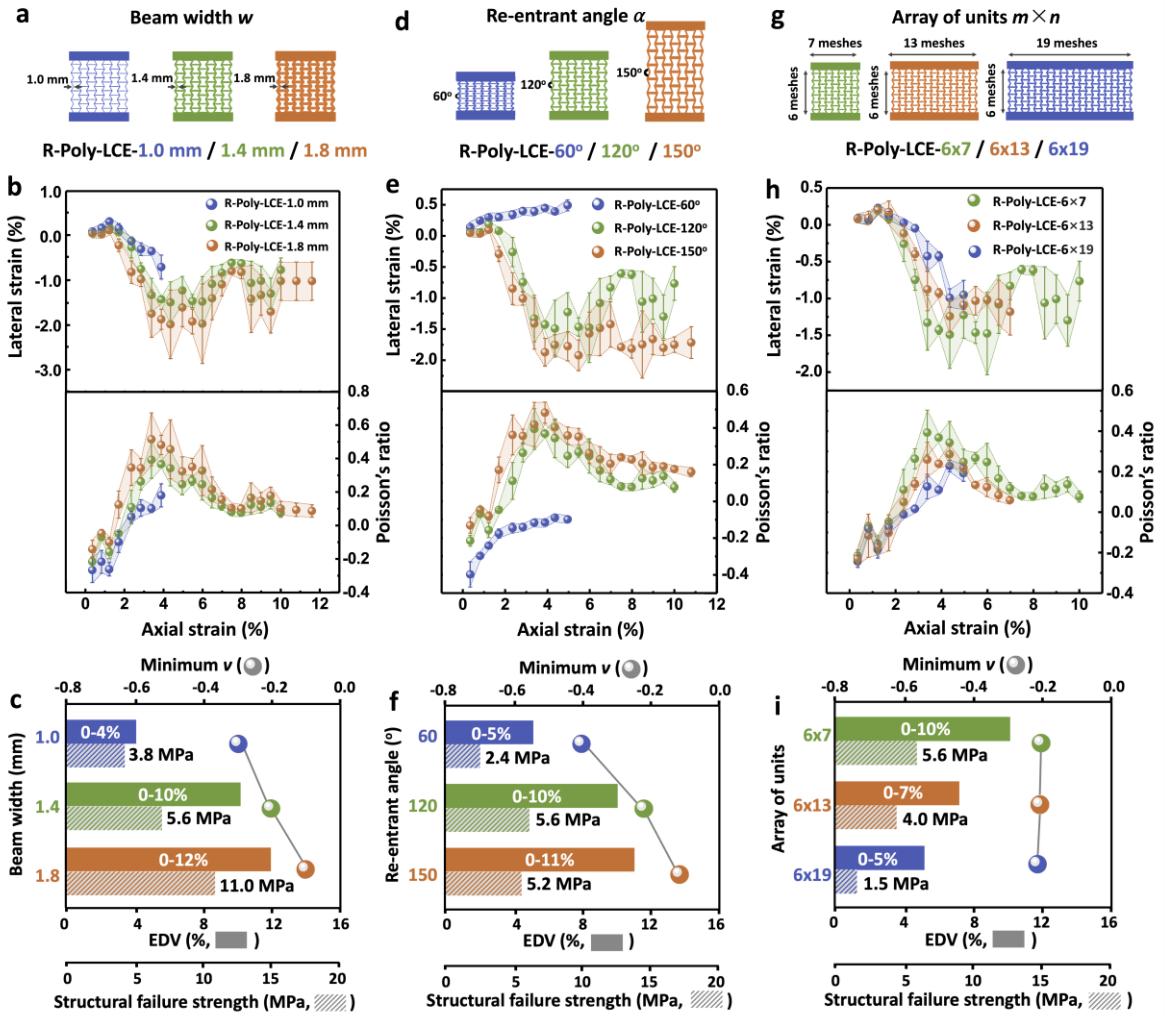

Figure 3. Geometric structure optimization of R-Poly-LCE. a) Diagram of R-Poly-LCE-1.0 mm, R-Poly-LCE-1.4 mm, and R-Poly-LCE-1.8 mm with different beam widths by fixing the angle of 120° and the array of units of 6×7. b) Variation of lateral strain and Poisson's ratio with axial strain of R-Poly-LCE-1.0 mm, R-Poly-LCE-1.4 mm, and R-Poly-LCE-1.8 mm, and c) the corresponding values of EDV, structural failure strength, and minimum Poisson's ratio. d) Diagram of R-Poly-LCE-60°, R-Poly-LCE-120°, and R-Poly-LCE-150° with different re-entrant angle by fixing the width of 1.4 mm and the array of units of 6×7. e) Variation of lateral strain and Poisson's ratio with axial strain of R-Poly-LCE-60°, R-Poly-LCE-120°, and R-Poly-LCE-150°, and f) the corresponding values of EDV, structural failure strength, and minimum

Poisson's ratio. g) Diagram of R-Poly-LCE-6×7, R-Poly-LCE-6×13, and R-Poly-LCE-6×19 with different unit arrays by fixing the width of 1.4 mm and the angle of 120°. h) Variation of lateral strain and Poisson's ratio with axial strain of R-Poly-LCE-6×7, R-Poly-LCE-6×13, and R-Poly-LCE-6×19, and i) the corresponding values of EDV, structural failure strength, and minimum Poisson's ratio. All error analysis is based on three test results.

2.4. Influence of liquid crystal orientation on Poisson's ratio

To investigate the influence of liquid crystal orientation on Poisson's ratio v of re-entrant LCE (R-LCE), we elaborated other two orientated R-LCE, namely R-Mono-LCE (//) and R-Mono-LCE (⊥), from Mono-LCE (//) and Mono-LCE (⊥) with the same geometric parameters of R-Poly-LCE. For R-Poly-LCE, the lateral extension occurred only when the elongation was smaller than 2% with a minimum v of -0.22. Extending the elongation from 2% to 10%, v first increased to 0.40, then decreased and tended to be stable at 0.10 (**Figure 4**a). For R-Mono-LCE (//), the minimum v (-0.12) also appeared at the beginning of the stretch, while swung around 0 as the stretch increased to 10% (Figure 4b). As for R-Mono-LCE (⊥), v increased from -0.16 and was gradually convergent to 0 with an increase of elongation to 3%, showing a similar convergence as R-Mono-LCE (//) (Figure 4c). By statistical analysis of Poisson's ratio distribution, it was found that both R-Mono-LCE (//) and R-Mono-LCE (⊥) showed a wider range of zero/negative Poisson's ratio ($v \leq 0$) during the stretching process. Compared with the elongation range where $v \leq 0$ in R-Poly-LCE (only at the beginning, 25% of the entire stretching process), R-Mono-LCE (//) and R-Mono-LCE (⊥) showed $v \leq 0$ in the whole elongation range before the structure failure, indicating better auxetic effect and zero-Poisson's ratio feature for the aligned LCE samples.

The stress distribution was mainly in the axial direction during the stretching process of R-LCE as confirmed by FEA analysis (Figure S17, Supporting Information). Thus, the original samples of R-Poly-LCE, R-Mono-LCE (//), R-Mono-LCE (⊥), and all samples stretched to an axial strain of 10% were characterized by 2D WAXS (Figure 4d, 4e, and 4f). Their intensity profiles as a function of q are shown in Figure S18 (Supporting Information). Clearly, orientation change occurs for all three samples after stretching as indicated by 2D WAXS patterns. In Figure 4d, the inner circular signal at q = 0.42 $Å^{-1}$ in the original R-Poly-LCE changes to two arc signals along the meridian. That means R-Poly-LCE initially polydomain without alignment tends to align with its smectic layer normally parallel to the stretching direction (meridian). This phenomenon is explained by the soft elasticity of Poly-LCE as discussed above (Figure 2e). The soft elasticity was also observed in R-Mono-LCE (//) and R-Mono-LCE (⊥) with orientations (Figure 2e). The stretching along the meridian caused the arc

signals of R-Mono-LCE (//) became sharper (Figure 4e middle) with the decrease of the full width at half-maximum (FWHM) of azimuthal profile of intensity (Figure 4e bottom and Figure S19, FWHM from 18.0° to 14.2°). It indicates the stretching along the orientation direction of R-Mono-LCE (//) can further enhance the orientation degree. In contrast, the stretching caused the arc signals of R-Mono-LCE (⊥) along the equator became larger (Figure 4f middle) with an increase of the FWHM of azimuthal profile of intensity (Figure 4f bottom and Figure S18, FWHM from 17.8° to 28.6°). That means the stretching weakens the orientation degree of R-Mono-LCE (⊥), because the stretching here tends to rotate the LC polymer chains.

The varying Poisson's ratios exhibited by R-LCEs with different orientation stem from the following reasons. (1) Within the 2% deformation range, the Poisson's ratio remains unaffected by the molecular configuration of all samples. The observed negative Poisson's ratio in this region is attributed to the alteration in the shape of the re-entrant structure. As the material is stretched, the re-entrant configuration prompts transverse expansion, concomitantly with an increase in its longitudinal dimension. This behavior induces strain in both longitudinal and vertical directions, resulting in a negative Poisson's ratio effect. (2) Within the 2% to 10% deformation range: For R-Poly-LCE, the flipping of liquid crystal units and the slipping between polymer chains facilitate transverse contraction during stretching. However, for R-Mono-LCE (//), it must overcome the competition between polymer chain slipping and internal stress under axial stretching, because the space for lateral deformation of polymer chains and liquid crystal units is limited. As a result, the lateral deformation remains close to zero in a finite space, and the range where $v \leq 0$ becomes wider. Distinct from R-Mono-LCE (//), since the stretching is perpendicular to the orientation direction in R-Mono-LCE (⊥), van der Waals force between polymer chains is initially overcome. But the force required to flip liquid crystal units is so substantial that it does not occur fully before the failure of R-Mono-LCE (⊥). Consequently, the lateral shrinkage is limited, and the Poisson's ratio tends towards 0.

In summary, R-Mono-LCE (//) and R-Mono-LCE (⊥) showed $v \leq 0$ at room temperature in the whole elongation range (10% strain) before the structure failure, which was in connection with their special soft elasticity. Benefiting from the orientation of liquid crystal polymer chains, R-Mono-LCE (//) and R-Mono-LCE (⊥) exhibited better auxetic effect with a wider range of $v \leq 0$.

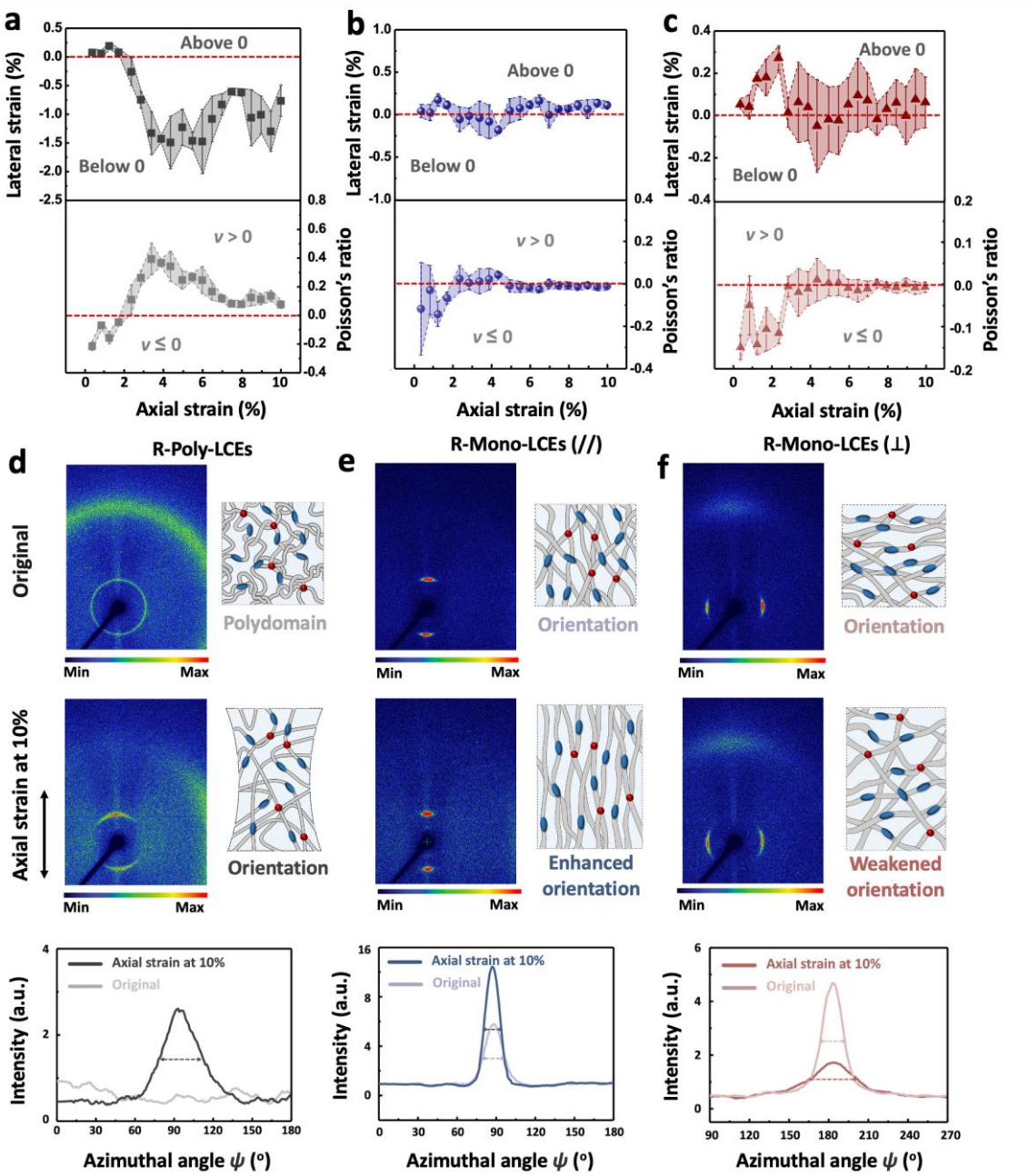

Figure 4. The influence of liquid crystal orientation on Poisson's ratio. The variation of lateral strain and Poisson's ratio as a function of axial strain for a) R-Poly-LCE, b) R-Mono-LCE (//), and c) R-Mono-LCE (⊥). All error analysis is based on three test results. 2D WAXS patterns of d) R-Poly-LCE, e) R-Mono-LCE (//), and f) R-Mono-LCE (⊥) (original samples and samples stretched with 10% axial strain) with the proposed rearrangements of molecular chains and azimuthal intensity profile of the inner signals at q = 0.42 $Å^{-1}$. The stretching was along the meridian. The azimuthal angle is set to 0° at lower part of equator (below the beam trap). The blue oval rod and the red sphere represent the LC units and the crosslinking point, respectively.

3. Conclusion

In this work, we have synthesized a main-chain Poly-LCE containing dynamic ester bonds, and its orientation process to Mono-LCE was greatly simplified by TERs-induced topological network rearrangements. Poly-LCE possessed the Young's modulus of 880 MPa and the fracture strength of 32.5 MPa at elongation of 136%. In contrast, when stretched along the long axis, the Young's modulus, fracture strength, and breaking elongation of Mono-LCE (//) were 1400 MPa, 66.4 MPa, and 28%, respectively, while those of Mono-LCE (⊥) were 640 MPa, 18.2 MPa, and 12%. Optimal geometric parameters with a beam of width 1.4 mm, re-entrant angle of 120^{o}, and array units of 6×7 have been determined through experiments and FEA. All samples of R-Poly-LCE, R-Mono-LCE (//), and R-Mono-LCE (⊥) with this re-entrant structure showed NPR effect below the elongation of 2%, ν = -0.22 ~ 0 for R-Poly-LCE, ν = -0.12 ~ 0 for R-Mono-LCE (//) and ν = -0.16 ~ 0 for R-Mono-LCE (⊥). Interestingly, R-Poly-LCE presented $\nu > 0$ when axial elongation ratio is from 2% to 10%, while R-Mono-LCE (//) and R-Mono-LCE (⊥) exhibited $\nu \approx 0$ under 2% to 10% stretching. Materials with negative and zero Poisson's ratios are interesting in niche applications. This work developed a simple method to prepare these materials by liquid crystal vitrimers capable of topological network rearrangements during the alignment by mechanical stretching. Meanwhile, it is worth noting that the vast majority of materials exhibiting negative Poisson's ratios rely on geometric pore structures. This effect can yield both positive and negative outcomes, contingent upon the application context and design objectives. Positive implications encompass weight reduction, enhanced breathability and drainage, energy absorption and cushioning, as well as heightened flexibility and deformability. Nonetheless, these materials also present drawbacks such as diminished strength and durability, along with limited environmental adaptability. Hence, the design and application of materials featuring negative Poisson's ratios necessitate a balanced consideration of their diverse impacts, tailored to specific requirements and environmental conditions.

Statistical Analysis

All data were obtained from at least three independent samples and expressed as the mean ± standard deviation (n = 3 for polymer characterization and mechanical studies).

Supporting Information

Supporting Information is available from the Wiley Online Library or from the author.

Acknowledgements

This work is supported by Beijing Natural Science Foundation (L233016) and the Open Research Fund of State Key Laboratory of Polymer Physics and Chemistry, Changchun Institute of Applied Chemistry, Chinese Academy of Sciences.

Conflict of Interest

The authors declare no conflict of interest.

Data Availability Statement

Research data are not shared.

Received: ((will be filled in by the editorial staff))
Revised: ((will be filled in by the editorial staff))
Published online: ((will be filled in by the editorial staff))

References

[1] C. Huang, L. Chen, *Adv. Mater.* **2016**, 28, 8079.

[2] N. I. Zheludev, *Science* **2010**, 328, 582.

[3] X. Guo, M. Guzmán, D. Carpentier, D. Bartolo, C. Coulais, *Nature* **2023**, 618, 506.

[4] W. Luo, X. Wang, X. Chen, S. Zheng, S. Zhao, Y. Wen, L. Li, J. Zhou, *Mater. Horiz.* **2023**, 10, 1769.

[5] Z. Zheng, J. Li, K. Wei, N. Tang, M.-H. Li, J. Hu, *Adv. Mater.* **2023**, 35, 2304631.

[6] R. H. Baughman, *Nature* **2003**, 425, 667.

[7] K. E. Evans, M. A. Nkansah, I. J. Hutchinson, S. C. Rogers, *Nature* **1991**, 353, 124.

[8] R. Lakes, *Science* **1987**, 235, 1038.

[9] G. N. Greaves, A. L. Greer, R. S. Lakes, T. Rouxel, *Nat. Mater.* **2011**, 10, 823.

[10] R. S. Lakes, *Annu. Rev. Mater. Res.* **2017**, 47, 63.

[11] Y. Jiang, Z. Liu, N. Matsuhisa, D. Qi, W. R. Leow, H. Yang, J. Yu, G. Chen, Y. Liu, C. Wan, Z. Liu, X. Chen, *Adv. Mater.* **2018**, 30, e1706589.

[12] X. Shi, Y. Zhu, X. Fan, H.-A. Wu, P. Wu, X. Ji, Y. Chen, J. Liang, *Matter* **2022**, 5, 1547.

[13] W. Xiong, R. Pan, C. Yan, M. He, Q. Chen, S. Li, X. Chen, L. Hao, Y. Li, *Addit. Manuf.* **2023**, 68, 103525.

[14] O. Skarsetz, V. Slesarenko, A. Walther, *Adv. Sci.* **2022**, 9, 2201867.

[15] C. Qi, F. Jiang, A. Remennikov, L.-Z. Pei, J. Liu, J.-S. Wang, X.-W. Liao, S. Yang, *Composites, Part B* **2020**, 197, 108117.

[16] X. Xu, Q. Zhang, M. Hao, Y. Hu, Z. Lin, L. Peng, T. Wang, X. Ren, C. Wang, Z. Zhao, C. Wan, H. Fei, L. Wang, J. Zhu, H. Sun, W. Chen, T. Du, B. Deng, G. J. Cheng, I. Shakir, C. Dames, T. S. Fisher, X. Zhang, H. Li, Y. Huang, X. Duan, *Science* **2019**, 363, 723.

[17] Q. Li, K. Lin, Z. Liu, L. Hu, Y. Cao, J. Chen, X. Xing, *Chem. Rev.* **2022**, 122, 8438.

[18] J. Küpfer, H. Finkelmann, *Die Makromol. Chem., Rapid Commun.* **1991**, 12, 717.

[19] D. L. Thomsen, P. Keller, J. Naciri, R. Pink, H. Jeon, D. Shenoy, B. R. Ratna, *Macromolecules* **2001**, 34, 5868.

[20] M.-H. Li, P. Keller, *Philos. Trans. R. Soc., A* **2006**, 364, 2763.

[21] M. Warner, E. M. Terentjev, *Liquid Crystal Elastomers*, Oxford University Press, Cambridge, United Kingdom **2003**.

[22] J. P. Cotton, F. Hardouin, *Prog. Polym. Sci.* **1997**, 22, 795.

[23] C. Song, Y. Zhang, J. Bao, Z. Wang, L. Zhang, J. Sun, R. Lan, Z. Yu, S. Zhu, H. Yang, *Adv. Funct. Mater*. **2023**, 33, 2213771.

[24] Y. Wang, Q. He, Z. Wang, S. Zhang, C. Li, Z. Wang, Y.-L. Park, S. Cai, *Adv. Mater.* **2023**, 35, 2211283.

[25] G. Liu, Y. Deng, B. Ni, G. T. M. Nguyen, C. Vancaeyzeele, A. Brulet, F. Vidal, C. Plesse, M.-H. Li, *Small* **2023**, 2307565.

[26] Z. Wang, Z. Wang, Y. Zheng, Q. He, Y. Wang, S. Cai, *Sci. Adv.* **2020**, 6, eabc0034.

[27] Y. Guo, J. Zhang, W. Hu, M. T. A. Khan, M. Sitti, *Nat. Commun.* **2021**, 12, 5936.

[28] D. J. Roach, X. Sun, X. Peng, F. Demoly, K. Zhou, H. J. Qi, *Adv. Funct. Mater.* **2022**, 32, 2203236.

[29] D. Mistry, S. D. Connell, S. L. Mickthwaite, P. B. Morgan, J. H. Clamp, H. F. Gleeson, *Nat. Commun.* **2018**, 9, 5095.

[30] L. Yin, L. Han, F. Ge, X. Tong,W. Zhang, A. Soldera, Y. Zhao, *Angew. Chem.,Int. Ed.* **2020**, 59, 15129.

[31] M. Barnes, S. M. Sajadi, S. Parekh, M. M. Rahman, P. M. Ajayan, R. Verduzco, *ACS Appl. Mater. Interfaces* **2020**, 12, 28692.

[32] T. Raistrick, Z. Zhang, D. Mistry, J. Mattsson, H. F. Gleeson, *Phys. Rev. Res.* **2021**, 3, 023191.

[33] Y. Huang, H. K. Bisoyi, S. Huang, M. Wang, X.-M. Chen, Z. Liu, H. Yang, Q. Li, *Angew. Chem., Int. Ed.* **2021**, 60, 11247.

[34] J. Chen, J. Jiang, J. Weber, V. Gimenez-Pinto, C. Peng, *ACS Appl. Mater. Interfaces* **2023**, 15, 4538.

[35] Z. Zhao, C. Yuan, M. Lei, L. Yang, Q. Zhang, H. Chen, H. J. Qi, D. Fang, *Phys. Rev. Appl.* **2019**, 11, 044074.

[36] H. M. A. Kolken, S. Janbaz, S. M. A. Leeflang, K. Lietaert, H. H. Weinans, A. A. Zadpoor, *Mater. Horiz.* **2018**, 5, 28.

[37] Y. Yao, E. He, H. Xu, Y. Liu, Z. Yang, Y. Wei, Y. Ji, *Nat. Commun.* **2023**, 14, 3518.

[38] B. Jin, S. Yang, *Adv. Funct. Mater.* **2023**, 33, 2304769.

[39] Z. Pei, Y. Yang, Q. Chen, E. M. Terentjev, Y. Wei, Y. Ji, *Nat. Mater.* **2014**, 13, 36.

[40] Y. Wu, Y. Yang, X. Qian, Q. Chen, Y. Wei, Y. Ji, *Angew. Chem,.Int. Ed.* **2020**, 59, 4778.

[41] J.-H. Lee, J. Bae, J. H. Hwang, M.-Y. Choi, Y. S. Kim, S. Park, J.-H. Na, D.-G. Kim, S.-k. Ahn, *Adv. Funct. Mater.* **2022**, 32, 2110360.

[42] J. N. Grima, L. Oliveri, D. Attard, B. Ellul, R. Gatt, G. Cicala, G. Recca, *Adv. Eng. Mater.* **2010**, 12, 855.

[43] T. Jin, N. S. Goo, S.-C. Woo, H. C. Park, *J. of Bionic Eng.* **2009**, 6, 224.

[44] G. Liu, J. Gao, L. Song, W. Hou, L. Zhang, *Macromol. Chem. Phys.* **2006**, 207, 2222.

[45] D. Montarnal, M. Capelot, F. Tournilhac, L. Leibler, *Science* **2011**, 334, 965.

[46] H. Gong, J. Wu, Z. Zhao, Z. Guo, L. Gao, B. Zhang, M.-H. Li, J. Hu, *Chem. Eng. J.* **2022**, 446, 137392.

[47] J.-H. Chen, B.-W. Liu, J.-H. Lu, P. Lu, Y.-L. Tang, L. Chen, Y.-Z. Wang, *Green Chem.* **2022**, 24, 6980.

[48] M. Chen, L. Zhou, Z. Chen, Y. Zhang, P. Xiao, S. Yu, Y. Wu, X. Zhao, *Compos. Sci. Technol.* 2022, 221, 109364.

[49] J. Wu, X. Yu, H. Zhang, J. Guo, J. Hu, M.-H. Li, *ACS Sustainable Chem. Eng.* 2020, 8, 6479.

[50] J. S. Biggins, M. Warner, K. Bhattacharya, *Phys. Rev. Lett.* **2009**, 103, 037802.

[51] E. M. Terentjev, *J. Phys.: Condens. Matter* **1999**, 11, R239.

[52] H. Finkelmann, A. Greve, M. Warner, *Eur. Phys. J. E* **2001**, 5, 281.

[53] K. M. Herbert, H. E. Fowler, J. M. McCracken, K. R. Schlafmann, J. A. Koch, T. J. White, *Nat. Rev. Mater.* **2022**, 7, 23.

[54] Z. Guo, X. Lu, X. Wang, X. Li, J. Li, J. Sun, *Adv. Mater.* **2023**, 35. 2300286.

[55] X. Wang, S. Zhan, Z. Lu, J. Li, X. Yang, Y. Qiao, Y. Men, J. Sun, *Adv. Mater.* **2020**, 32, 2005759.

[56] T. Guan, X. Wang, Y.-L. Zhu, L. Qian, Z. Lu, Y. Men, J. Li, Y. Wang, J. Sun, *Macromolecules* **2022**., 55, 13.

[57] R. S. Lakes, *Annu. Rev. Mater. Res.* **2017**, 47, 6.

[58] X. C. Teng, X. Ren, Y. Zhang, W. Jiang, Y. Pan, X. G. Zhang, X. Y. Zhang, Y. M. Xie, *Int. J. Mech. Sci.* **2022**, 229, 107524.

[59] J. Valente, E. Plum, I. J. Youngs, N. I. Zheludev, *Adv. Mater.* **2016**, 28, 5176.

[60] J. Hao, D. Han, X. G. Zhang, Y. Zhang, W. Jiang, X. C. Teng, J. P. Lang, Y. Pan, X. H. Ni, X. Y. Zhang, Y. M. Xie, X. Ren, *Eng. Struct.* 2022, 270, 114891.